# **ARTICLE**

# Tandem catalysis using an enzyme and a polymeric rutheniumbased artificial metalloenzyme

Received 00th January 20xx, Accepted 00th January 20xx

DOI: 10.1039/x0xx00000x

Edzna S. Garcia, a Thao M. Xiong, a Abygail Lifschitz, a and Steven C. Zimmerman\*a

A Ru-containing single chain nanoparticle (SCNP) was prepared in three steps using radical polymerization of pentafluorophenylacrylate, post-polymerization functionalization with three different alkylamines, and coordination of Ru. The polymer was characterized by  $^1$ H NMR,  $^{19}$ F NMR, UV-vis, and DLS. The catalytic activity of the Ru-SCNP for Ru-catalyzed cleavage of allylcarbamates was evaluated by fluorescence spectroscopy and higher percent conversion and initial rate of reaction was observed when compared to that of the free catalyst in buffer and cell media. The catalytic SCNP was also shown to perform tandem catalysis with  $\beta$ -galactosidase.

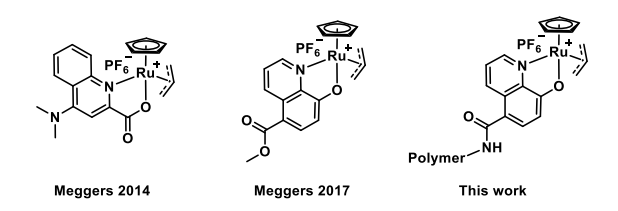
#### Introduction

Water is considered the most environmentally benign solvent for organic synthesis.<sup>1,2</sup> Thus, it comes as no surprise that considerable effort has been invested in developing synthetic transformations without the need for organic solvents. Performing transition metal catalysis in water is of particular interest because of the potential application in bioorthogonal transformations relating to bioconjugation reactions,<sup>3-5</sup> cell surface modifications,<sup>6-8</sup> and in situ drug synthesis.<sup>9-15</sup> However, many transition metal catalysts are not water soluble and their activity in water is compromised.

Polymer scaffolds have been used to improve the compatibility, longevity, and overall performance of transition metal catalysts in water and biorelevant conditions. 10,13,16-19 The polymeric scaffolds can serve various functions, including their ability to impart water solubility, enhance catalyst stability in environments that would otherwise deactivate them, and provide pockets for substrate binding thereby allowing low concentration reactions to proceed with serviceable rates. These characteristics of catalytic SCNPs make them an important new class of reagents for chemical biology, and more specifically for performing bioorthogonal reactions. More broadly, the use of the transition metal catalysts greatly expands the range of chemical transformations that can be performed in biological systems. Applications to date include in cellulo or in vivo drug synthesis, 10-15 unmasking of pro-drugs, 9,12 and biomacromolecule labelling.3-5

Meggers and coworkers have developed several nonpolymeric ruthenium catalysts that promote the uncaging of alloc protected amines in aqueous media and inside living cells.<sup>20,21</sup> The initial work featured a Kitamura catalyst with a 2-quinolinecarboxylate ligand that was shown to work well in cells.<sup>20</sup> In 2017 Meggers and Volker reported an 8-hydroxy-quinolate Ru complex with improved catalytic activity and low cell toxicity.<sup>21</sup>

Given the demonstrated biocompatibility of these catalysts, we wondered if covalent linking one to a polymer would further



improve its properties, especially allowing enzyme-like substrate binding. Further, our previous work clickases  $^{8,10,13,18}$  and photoreductases  $^{19}$  used SCNPs that were covalently cross-linked with the metal ligand or the metal itself. To streamline the preparation of the SCNP, we sought to covalently attach the metal ligand by a single attachment and to use the collapse of the hydrophobic interior to form the nanoparticle. Finally, we recently described19 an example of intracellular synthesis that involved tandem catalysis with the coupling of an SCNP-based artificial enzyme with a natural enzyme. Tandem catalysis in biological relevant conditions is a very exciting and important step toward more complex in-cell therapeutic synthesis. Indeed, a few examples have already been reported. 19,22,23 Herein, we test in aqueous solution several of these ideas using a ruthenium containing single-chain nanoparticle (SCNP) formed from a random amphiphilic copolymer.

<sup>&</sup>lt;sup>a</sup>Department of Chemistry, University of Illinois at Urbana-Champaign, Urbana, Illinois 61801, United States.

E-mail: sczimmer@illinois.edu

<sup>†</sup>Electronic Supplementary Information (ESI) available: [details of any supplementary information available should be included here]. See DOI: 10.1039/x0xx00000x

ARTICLE Journal Name

Fig. 1. Ru-P1 was synthesized via post-polymerization functionalization of pPFPA with quinoline 1, naphthalene 2, and Jeffamine M-1000 followed by Ru coordination.

#### Results and discussion

#### Synthesis of polymers

Random amphiphilic copolymer P1 was prepared as outlined in Fig. 1, beginning with poly(pentafluorophenyl acrylate) (pPFPA<sub>100</sub>), which was prepared by reversible additionfragmentation chain-transfer (RAFT) polymerization following a reported procedure.<sup>24</sup> The activated ester groups of pPFPA readily undergo substitution reactions with amines, providing a convenient way to obtain functional polymers by postpolymerization functionalization. Thus, the polyacrylamide P1 was obtained by amine functionalization of pPFPA100 with sequential addition of quinoline 1, naphthalene 2, and Jeffamine M-1000 in THF/DMF at 50 °C in the presence of DIPEA. The general synthetic approach follows from an approach developed by Palmans, Meijer, and coworkers. 17 The amounts of each amine were carefully controlled to obtain a functionalization ratio of 20:30:50 of 1:2:Jeffamine M-1000, respectively. This particular graft ratio and the choice of hydrophobic amine 2 was guided by a quick screen of the ultimate catalysts that indicated SCNP derived from 2 performed better than those based on dodecylamine and that 30% naphthyloxyhexyl units gave a higher rate and conversion than did 20% or 40% (vide infra). The design of 2 was based on the observation that proteins have both aliphatic and aromatic side-chains. Thus, we chose to explore a group that contains both segments. The aromatic group provides a more polar microenvironment that may be useful to the catalytic process.

The progress of the amine grafting reaction was monitored by  $^{19}\text{F}$  NMR (Fig. S1). The percent conversion was calculated from the ratio of the peak integrations of fluorine signals from

the released pentafluorophenol and that of **pPFPA**<sub>100</sub>. The observed percent conversions of 23%, 34%, and 43% are consistent with the feed ratio of **1**, **2**, and Jeffamine M-1000, respectively. Polymer **P1** was further characterized by size-exclusion chromatography (SEC) in DMF with 0.1 M LiBr to obtain a molecular weight ( $M_n$ ) of 54.8 kDa and a low dispersity ( $M_w/M_n$ ) of 1.2.

Polymer **Ru-P1** was obtained by treating **P1** with [CpRu(MeCN)<sub>3</sub>]PF<sub>6</sub> in MeCN, Ru coordination to the quinoline ligands<sup>21</sup> and the reaction progress was readily monitored via <sup>1</sup>H NMR (Fig. 2). The allyl protons of quinoline side chain **1** experienced an upfield chemical shift, which indicates

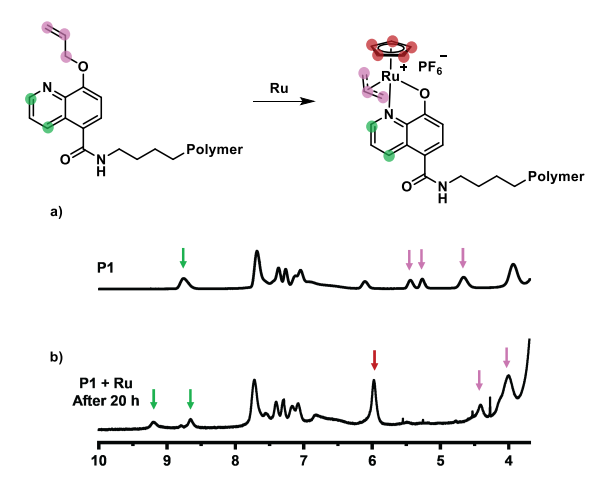


**Fig. 2.** <sup>1</sup>H NMR in CD<sub>3</sub>CN of a) **P1** before and b) after addition of Ru. The resolution of quinoline protons (green arrows), appearance of a cyclopentadienyl peak (red arrow), and upfield shift of the allyl protons on the ligand (pink arrows) were observed 20 h after addition of Ru.

Journal Name ARTICLE

coordination to the electron dense Ru center. In addition, the appearance of a broad cyclopentadienyl peak at  $\delta$  6 ppm and resolution of the quinoline protons at  $\delta$  9 ppm were observed. These proton chemical shifts are consistent with those observed for the quinoline and allyl groups in the small catalyst model **Ru1** (Fig. S2).

#### Quantification of catalyst loading

To quantify the efficiency of the Ru coordination to **P1**, small molecule models **3** and **Ru1** were synthesized (Fig. 3a). **P1**, **Ru-P1**, and the small molecule models were characterized by UV-vis spectroscopy in MeCN (Fig. 3b,c). Ligands **3** and polymer **P1** have absorption bands below 350 nm. Small molecule catalyst model **Ru1** has an absorption band at  $\lambda_{max} = 401$  nm, which corresponds to the metal-to-ligand charge transfer (MLCT) process. <sup>25</sup> This MLCT band was also observed for **Ru-P1** and was used to quantify the concentration of catalyst loading after Ru coordination to **P1**. A calibration curve was generated from the UV-vis spectra of **Ru1** at various concentrations ranging from 5  $\mu$ M to 200  $\mu$ M (Fig. S3). Based on the calibration curve and the  $M_n$  of **P1**, it is calculated that **Ru-P1** contains approximately 15 Ru per polymer chain.

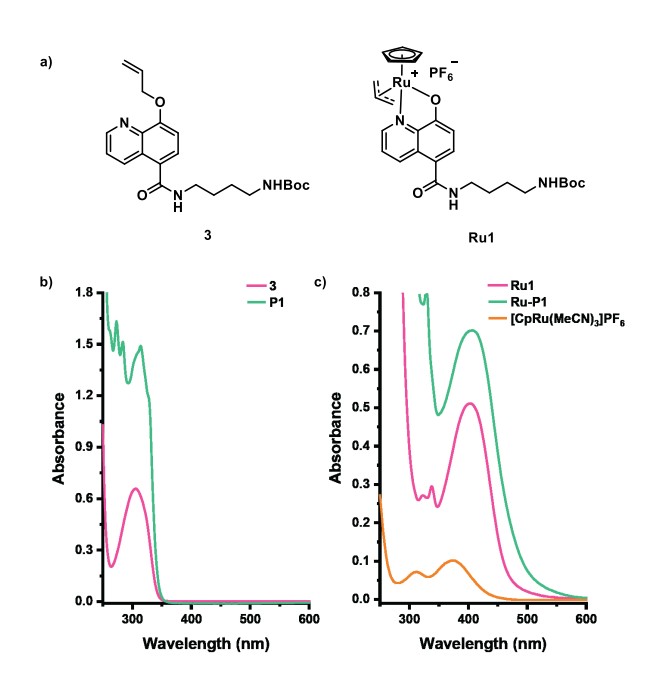


**Fig. 3.** a) Structure of small molecule models **3** and **Ru1**, and UV-Vis spectra in MeCN of b) **3** (100  $\mu$ M) and **P1** (0.5 mg/mL, 9.1  $\mu$ M) and c) **Ru1** (100  $\mu$ M), **Ru-P1** (138  $\mu$ M Ru), and [CpRu(MeCN)<sub>3</sub>]PF<sub>6</sub> (100  $\mu$ M).

### **Characterization of polymers**

In water, amphiphilic random copolymers such as **P1** and **Ru-P1** may intramolecularly fold into the desired SCNP or intermolecularly aggregate to form micelles. <sup>26-29</sup> The Sawamoto and Terashima groups have extensively studied the self-assembly of amphiphilic random copolymers into unimolecular micelles in water. <sup>30-32</sup> Because our polymers are not covalently

crosslinked, their ability to form a SCNP is similarly concentration dependent. We sought to determine the critical micelle concentration (CMC) of P1 and Ru-P1 in PBS by observing their ability to encapsulate Nile Red, a fluorescent probe that exhibits low fluorescence in aqueous environments but has a dramatic increase in fluorescence intensity when the dye inhabits a hydrophobic environment.33-35 The fluorescence emission of Nile Red in PBS was measured in the presence of concentrations of P1 and Ru-P1 ranging from 0.5  $\mu g/mL$  (9.1 nM) to 1.0 mg/mL (18.2  $\mu$ M) (Fig. 4). The CMC value for **P1** was calculated as approximately  $0.025 \pm 0.003$  mg/mL ( $456 \pm 55$  nM, average of two independent studies and standard error is reported). We were unable to determine a CMC value for Ru-P1 due to an interference of the dye fluorescence by the Rucomplex. Characterization by dynamic light scattering (DLS) indicated a hydrodynamic diameter of 8.1 ± 1.3 nm and 8.6 ± 0.6 nm for P1 and Ru-P1, respectively when measured at 0.1 mg/mL or 1.8 μM (Fig. S4). When measured around the CMC value at 0.02 mg/mL (365 nm) the hydrodynamic diameters are  $9.6 \pm 0.5$  nm and  $10.6 \pm 0.5$  nm for **P1** and **Ru-P1** respectively. Because the particles form from the intramolecular chain folding without covalent bonds, some variation in size is expected. This size is consistent with what has been reported in the literature for copolymers with similar molecular weight.<sup>36</sup>

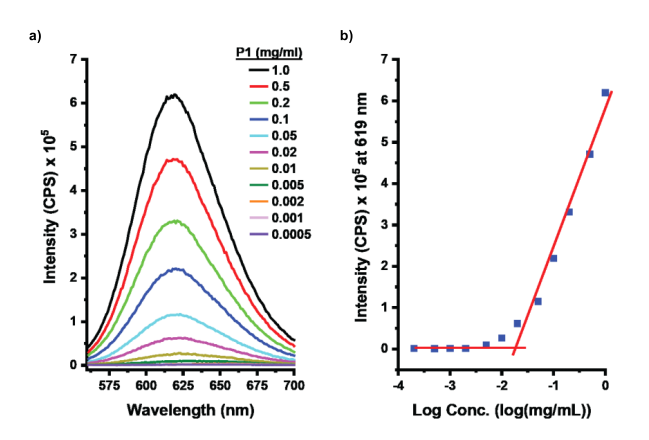
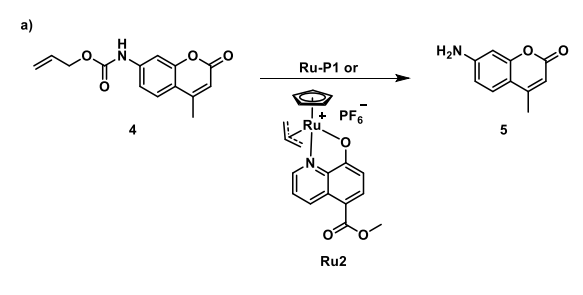


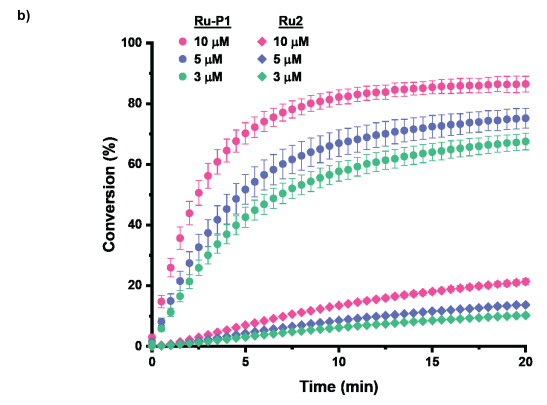
**Fig. 4.** a) Critical micelle concentration study by encapsulation of Nile Red (1  $\mu$ M) by **P1** in 10 mM PBS pH 7.4 at  $\lambda_{ex}$  = 553 nm. Fluorescence emission spectra were recorded from 561-700 nm. b) Fluorescence emission intensities at 619 nm were extracted and plotted.

#### Ru-catalyzed cleavage of allylcarbamates

Next, we compared the activity of **Ru-P1** to previously reported free catalyst **Ru2**. We expected that the polymeric system would provide an advantage by supporting substrate binding and creating a higher local concentration of substrate and catalyst thus enhancing catalysis compared to a small molecule catalyst.<sup>8,18</sup> The catalytic activity of **Ru-P1** and **Ru2** for Ru-catalyzed cleavage of allylcarbamates was analysed using fluorescence spectroscopy. Caged coumarin **4** is non-fluorescent, but decaged amine **5** is fluorescent (Fig. 5a).<sup>37</sup> The

ARTICLE Journal Name





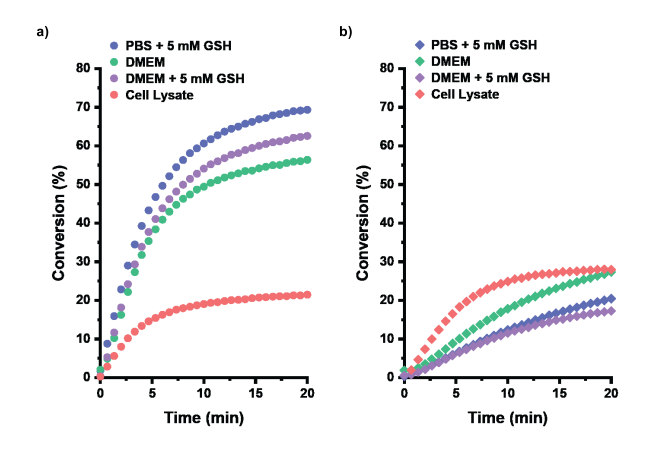
|      |      | Ru-P1  |            | R             | lu2        |
|------|------|--------|------------|---------------|------------|
| Ru   | 4    | Rate   | Conversion | Rate          | Conversion |
| (μM) | (μM) | (nM/s) | (%)        | (nM/s)        | (%)        |
| 10   | 20   | 72 ± 9 | 86 ± 3     | 5.0 ± 0.2     | 21 ± 1     |
| 5    | 20   | 42 ± 7 | 75 ± 3     | $3.3 \pm 0.1$ | 14 ± 1     |
| 3    | 20   | 33 ± 4 | 68 ± 3     | 2.2 ± 0.1     | 10.3 ± 0.3 |

**Fig. 5.** Fluorescence studies of Ru-catalyzed cleavage of allylcarbamates using **Ru-P1** (circle) and small molecule **Ru2** (diamond) at different concentrations of Ru. [GSH] = 300  $\mu$ M, in PBS 1x, room temp,  $\lambda_{ex}$  = 375 nm,  $\lambda_{em}$  = 440 nm.

study was performed at room temperature in PBS buffer containing 300  $\mu M$  glutathione (GSH, which was used by Meggers and coworkers²¹) with a fixed concentration of **4** (20  $\mu M$ ) while varying the concentration of **Ru-P1** and **Ru2**, and the reaction progress was monitored by the increase in fluorescence emission over 20 min (Fig. 5b). We used Ru concentrations of 10, 5 and 3  $\mu M$ , which for **Ru-P1** are concentrations that are above (830 nM), at (415 nM), and below (248 nM) the CMC, respectively. Initial rates and percent conversions increase with increasing Ru concentration. Overall, higher percent conversions and faster initial rates of reactions were observed with **Ru-P1** compared with the small molecule model **Ru2**.

The performance of **Ru-P1** and **Ru2** was also investigated in biologically relevant conditions. The allylcarbamate cleavage reactions were performed in PBS containing 5 mM GSH, Dulbecco's Modified Eagle Medium (DMEM), and DMEM containing 5 mM GSH (Fig. 6). Under these conditions, **Ru-P1** achieved conversions of 56-69% and initial rates of 28-35 nM/s. On the other hand, conversions of 17-27% and initial rates of 4-

6 nM/s were observed for small molecule catalyst Ru2 under the same biologically relevant conditions. In addition, the catalytic activity of Ru-P1 and Ru2 was assessed in HeLa cell lysate to probe their ability to perform in complex biological environments. Slower initial rates and lower percent conversions were observed for Ru-P1 catalysed reactions carried out in cell lysate. This was expected due to the complex environment off cell lysate. In general, Ru-P1 exhibited faster initial rates and higher conversions than Ru2 in all the reactions carried out in PBS and DMEM. However, Ru-P1 and Ru2 have similar initial rates and conversions in cell lysate. The lower activity of Ru-P1 compared to Ru2 in cell lysate suggests a reduced ability to bind substrates and provide a protective environment for the catalyst, potentially due to unfolding of the polymer chain that enhances interactions with specific cellular biomacromolecules. However, additional studies would be needed to determine the origin of this observation.



|                    |                | Ru-P1             | Ru2            |                   |  |
|--------------------|----------------|-------------------|----------------|-------------------|--|
| Conditions         | Rate<br>(nM/s) | Conversion<br>(%) | Rate<br>(nM/s) | Conversion<br>(%) |  |
| PBS + 5 mM GSH     | 35 ± 6         | 69 ± 4            | 4 ± 1          | 20 ± 3            |  |
| DMEM               | 28 ± 3         | 56 ± 3            | 6 ± 1          | 27 ± 2            |  |
| DMEM + 5 mM<br>GSH | 30 ± 1         | 62 ± 3            | 3.9 ± 0.3      | 17 ± 1            |  |
| Lysate             | 12 ± 1         | 21 ± 3            | 12 ± 1         | 28 ± 1            |  |

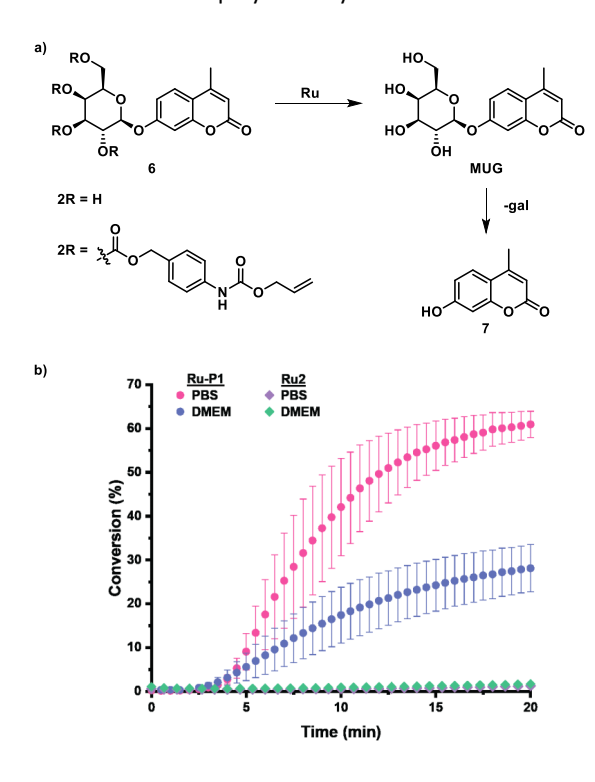
**Fig. 6.** Fluorescence studies of Ru-catalyzed cleavage of allylcarbamates using a) **Ru-P1** and b) **Ru2** with or without 5 mM GSH. [4] = 20  $\mu$ M, [**Ru-P1**] or [**Ru2**] = 5  $\mu$ M in Ru, in PBS 1x or DMEM, room temp,  $\lambda_{ex}$  = 375 nm,  $\lambda_{em}$  = 440 nm. For clarity, error bars are not shown but can be found in Fig S5.

# **Tandem Catalysis**

We have demonstrated the polymer's ability to improve the catalytic activity of Ru in PBS and DMEM. Next, we explored the capacity of **Ru-P1** to perform tandem catalysis with a native enzyme. The combination of synthetic chemistry by the artificial metalloenzyme with biocatalysis provides important new synthetic strategies for chemical biology. The enzyme  $\beta$ -galactosidases ( $\beta$ -gal) is an essential enzyme that is commonly

Journal Name ARTICLE

used in chemical biology.<sup>38</sup> We have recently shown that  $\beta$ -gal is compatible with a photocatalyst to perform intracellular tandem catalysis.<sup>19</sup> We explored the compatibility of **Ru-P1** to perform tandem catalysis with  $\beta$ -gal. For this, we designed substrate **6**, a 4-methylumbelliferyl  $\beta$ -D-galactopyranoside (MUG) derivative where two hydroxyl groups are randomly protected with allylcarbamate phenyl carbonate groups. The catalysis starts with two allylcarbamate cleavage reactions catalysed by **Ru-P1**. This generates aniline groups that undergo a 1,6-type elimination and decarboxylation to release MUG, which serves as a substrate for  $\beta$ -gal releasing fluorescent coumarin **7** (Fig. 7a). This type of quinone-methide elimination has been used as a tool in prodrug activation, diagnostic probes, and self-immolative polymeric systems.<sup>39</sup>



|            | Ru-P1          |        | Ru2 |                   |
|------------|----------------|--------|-----|-------------------|
| Conditions | Rate<br>(nM/s) |        |     | Conversion<br>(%) |
| PBS        | 32 ± 6         | 61 ± 3 | < 1 | < 2               |
| DMEM       | 10 ± 3         | 28 ± 5 | < 1 | < 2               |

**Fig. 7.** a) Tandem reaction conducted with **Ru-P1** and β-gal, b) fluorescence studies of tandem catalysis using **Ru-P1** and **Ru2** with β-gal. [Ru] = 5  $\mu$ M, [6] = 20  $\mu$ M, in PBS 1x or DMEM, room temp,  $\lambda_{ex}$  = 340 nm,  $\lambda_{em}$  = 445 nm.

The tandem catalysis was performed in PBS and DMEM with 5  $\mu$ M of Ru and 20  $\mu$ M of substrate 6. Ru-P1 achieved 69% conversion and an initial rate of 3 nM/s in PBS and 28% conversion and an initial rate of 10 nM/s in DMEM. In contrast, the reactions catalysed by Ru2 only reached 1-2% conversion

after 20 min. Because of these low conversions the rates for **Ru2** were not calculated.

#### Conclusions

In conclusion, we have reported a Ru-containing SCNP Ru-P1 that does not require covalent crosslinking to enhance catalysis in PBS and DMEM. Under these conditions, Ru-P1 outperforms the free catalyst for the Ru catalysed cleavage of allylcarbamate groups. We have also demonstrated its ability to perform tandem catalysis with a natural enzyme to unlock a double gated system to release a fluorescent probe. This simple strategy to obtain functional SCNPs has the potential to be applied to other SCNP-based transition metal catalysts. Indeed, eliminating the cross-linking steps should streamline the development of such catalysts while further expanding the chemist's toolbox for transition metal catalysis in aqueous environments.

#### **Author Contributions**

The manuscript was written through contributions of all authors. All authors have given approval to the final version of the manuscript.

#### **Conflicts of interest**

The authors declare no conflicts of interest.

# **Acknowledgements**

The authors gratefully acknowledge financial support from the National Science Foundation (NSF CHE-1709718) and Sarah Krueger for providing the cell lysate.

#### Notes and references

- C. J. Li and B. M. Trost, Proc. Natl. Acad. Sci. USA, 2008, 105, 13197-13202.
- T. Kitanosono, K. Masuda, P. Y. Xu and S. Kobayashi, *Chem. Rev.*, 2018, **118**, 679-746.
- (3) J. M. Chalker, G. J. L. Bernardes and B. G. Davis, Acc. Chem. Res., 2011, 44, 730-741.
- (4) J. M. Antos and M. B. Francis, Curr. Opin. Chem. Biol., 2006, 10, 253-262.
- (5) W. M. Cheng, X. Lu, J. Shi and L. Liu, *Org. Chem. Front.*, 2018,5, 3186-3193.
- (6) J. Wang, B. Cheng, J. Li, Z. Y. Zhang, W. Y. Hong, X. Chen and P. R. Chen, Angew. Chem. Int. Edit., 2015, 54, 5364-5368.
- B. Ovryn, J. Li, S. L. Hong and P. Wu, Curr. Opin. Chem. Biol., 2017, 39, 39-45.
- (8) J. F. Chen, J. Wang, K. Li, Y. H. Wang, M. Gruebele, A. L. Ferguson and S. C. Zimmerman, J. Am. Chem. Soc., 2019, 141, 9693-9700.
- (9) G. Y. Tonga, Y. D. Jeong, B. Duncan, T. Mizuhara, R. Mout, R. Das, S. T. Kim, Y. C. Yeh, B. Yan, S. Hou and V. M. Rotello, *Nat. Chem.*, 2015, 7, 597-603.

ARTICLE Journal Name

- (10) Y. G. Bai, X. X. Feng, H. Xing, Y. H. Xu, B. K. Kim, N. Baig, T. H. Zhou, A. A. Gewirth, Y. Lu, E. Oldfield and S. C. Zimmerman, J. Am. Chem. Soc., 2016, 138, 11077-11080.
- (11) J. Clavadetscher, S. Hoffmann, A. Lilienkampf, L. Mackay, R. M. Yusop, S. A. Rider, J. J. Mullins and M. Bradley, *Angew. Chem. Int. Edit.*, 2016, **55**, 15662-15666.
- (12) A. M. Perez-Lopez, B. Rubio-Ruiz, V. Sebastian, L. Hamilton, C. Adam, T. L. Bray, S. Irusta, P. M. Brennan, G. C. Lloyd-Jones, D. Sieger, J. Santamaria and A. Unciti-Broceta, Angew. Chem. Int. Edit., 2017, 56, 12548-12552.
- (13) J. F. Chen, K. Li, S. E. Bonson and S. C. Zimmerman, *J. Am. Chem. Soc.*, 2020, **142**, 13966-13973.
- (14) D. P. Nguyen, H. T. H. Nguyen and L. H. Do, ACS Catal., 2021,11, 5148-5165.
- (15) T. C. Chang and K. Tanaka, Bioorg. Med. Chem. 2021, 46, 116353.
- M. Artar, E. R. J. Souren, T. Terashima, E. W. Meijer and A.
  R. A. Palmans, ACS Macro. Lett., 2015, 4, 1099-1103.
- (17) Y. L. Liu, S. Pujals, P. J. M. Stals, T. Paulohrl, S. I. Presolski, E. W. Meijer, L. Albertazzi and A. R. A. Palmans, *J. Am. Chem. Soc.*, 2018, **140**, 3423-3433.
- (18) J. F. Chen, J. Wang, Y. G. Bai, K. Li, E. S. Garcia, A. L. Ferguson and S. C. Zimmerman, J. Am. Chem. Soc., 2018, 140, 13695-13702.
- (19) J. F. Chen, K. Li, J. S. Shon and S. C. Zimmerman, *J. Am. Chem. Soc.*, 2020, **142**, 4565-4569.
- (20) T. Volker, F. Dempwolff, P. L. Graumann and E. Meggers, Angew. Chem. Int. Edit., 2014, 53, 10536-10540.
- (21) T. Volker and E. Meggers, ChemBioChem, 2017, 18, 1083-1086.
- (22) F. Rudroff, M. D. Mihovilovic, H. Groger, R. Snajdrova, H. Iding and U. T. Bornscheuer, Nat. Catal., 2018, 1, 12-22.
- (23) V. Kohler, Y. M. Wilson, M. Durrenberger, D. Ghislieri, E. Churakova, T. Quinto, L. Knorr, D. Haussinger, F. Hollmann, N. J. Turner and T. R. Ward, *Nat. Chem.*, 2013, 5, 93-99.

- (24) A. Das and P. Theato, *Macromolecules*, 2015, **48**, 8695-8707.
- (25) J. Bonvoisin and I. Ciofini, *Dalton. Trans.*, 2013, **42**, 7943-7951.
- (26) S. Mavila, O. Eivgi, I. Berkovich and N. G. Lemcoff, *Chem. Rev.*, 2016, **116**, 878-961.
- (27) Pomposo, J. A., Ed. Single-Chain Polymer Nanoparticles: Synthesis, Characterization, Simulations, and Applications; John Wiley & Sons, 2017.
- (28) R. W. Chen and E. B. Berda, ACS Macro. Lett., 2020, 9, 1836-1843.
- (29) M. H. Barbee, Z. M. Wright, B. P. Allen, H. F. Taylor, E. F. Patteson and A. S. Knight, *Macromolecules*, 2021, 54, 3585-3612.
- (30) T. Terashima, T. Sugita, K. Fukae and M. Sawamoto, Macromolecules, 2014, 47, 589-600.
- (31) G. Hattori, Y. Hirai, M. Sawamoto and T. Terashima, *Polym. Chem.*, 2017, **8**, 7248-7259.
- (32) M. Shibata, M. Matsumoto, Y. Hirai, M. Takenaka, M. Sawamoto and T. Terashima, *Macromolecules*, 2018, **51**, 3738-3745.
- (33) S. D. Fowler and P. Greenspan, J. Histochem. Cytochem., 1985, 33, 833-836.
- (34) P. Greenspan, E. P. Mayer and S. D. Fowler, *J. Cell Biol.*, 1985, **100**, 965-973.
- (35) M. C. A. Stuart, J. C. van de Pas and J. B. F. N. Engberts, J. Phys. Org. Chem., 2005, 18, 929-934.
- (36) Y. L. Liu, T. Pauloehrl, S. I. Presolski, L. Albertazzi, A. R. A. Palmans and E. W. Meijer, J. Am. Chem. Soc., 2015, 137, 13096-13105.
- Y. Kanaoka, T. Takahashi, H. Nakayama, T. Ueno and T. Sekine, Chem. Pharm. Bull., 1982, 30, 1485-1487.
- (38) D. H. Juers, B. W. Matthews and R. E. Huber, *Protein Sci.* 2012, 21, 1792–1807.
- (39) S. Gnaim and D. Shabat, *Acc. Chem. Res.*, 2014, **47**, 2970-2984.